

# Development of a Laser Based Process Chain for Manufacturing Free Form Optics

S. Heidrich<sup>\*a</sup>, A. Richmann<sup>b</sup>, Dr. E. Willenborg<sup>a</sup>

<sup>a</sup>Fraunhofer Institute for Laser Technology ILT, Steinbachstr. 15, 52074 Aachen, Germany

<sup>b</sup>Chair for the Technology of Optical Systems TOS, RWTH Aachen University, Steinbachstr. 15,  
52074 Aachen, Germany

## ABSTRACT

This paper presents the development of a laser based process chain for manufacturing fused silica optics. Due to disadvantages of conventional methods concerning costs and time when manufacturing optics with nonspherical shape, this process chain focuses on aspherical and free form surface geometries, but it is also capable of producing spherical optics. It consists of three laser based processing steps, which in combination produce the optics. In a first step, fused silica is ablated with laser radiation to produce the geometry of the optics. A subsequent laser polishing step reduces the surface roughness and a third step uses laser micro ablation to remove the last remaining redundant material. Most of the conducted experiments are carried out using CO<sub>2</sub> laser radiation, but it is also possible to ablate material with ultra short pulse laser radiation. Besides describing the experimental setup and the mechanisms of the ablation and polishing step, the paper presents and discusses results achieved to date. Although the process chain is still under development, the single process steps already reach promising results for themselves and moreover, first elements are manufactured using the first two process steps together.

**Keywords:** glass, fused silica, optics, aspherical, free form, laser, process chain, polishing

## 1. INTRODUCTION

Increasing demands of modern optical components concerning imaging quality, functionality and lightweight affect both products of the mass market such as spectacle glasses as well as specialized optics such as lenses for lasers. Aspherical or freeform optics are more expensive to produce but can substitute two or more spherical lenses and thus lower the size and the weight of products.

One conventional method for manufacturing optical components is grinding and polishing. Starting from a preform, several grinding steps create the surface shape of the resulting optics by removing material. Thereby, each step uses smaller abrasive grain in order to reduce the surface damage induced by the previous grinding steps. The same procedure is used for the following polishing steps. Because of the many grinding and polishing steps, this method has disadvantages regarding the production time, especially when manufacturing nonspherical optics due to the required zonal polishing [1].

Another method for manufacturing optical components is glass precision molding which is used especially for large numbers of identical optics. In this process, glass is pressed into a casting mold which then forms the optics without any further treatment. According to the casting mold's surface form, this method is capable of producing spherical as well as aspherical or free form optics, but the fabrication of the casting mold is costly in terms of money and time, because it needs a precise shape which directly forms the optics surface. Moreover, glasses with a high softening temperature like fused silica cannot be processed due to the limited thermal stability of the casting mold [1].

So, the production of single pieces or small series of aspherical or free form optics with conventional manufacturing methods is generally very expensive. The aim of the process chain presented here is to increase the flexibility and individualization in the manufacturing of optical components by using laser radiation. This includes the processing of the geometry as well as the polishing step. Without the use of form-giving tools, especially aspheres and free form optics can be manufactured with high flexibility and short lead time. The process chain, its process steps and first results are described in the next chapters.

\*sebastian.heidrich@ilt.fraunhofer.de; phone +49 241 8906-645; fax +49 241 8906-121; <http://www.ilt.fraunhofer.de>

## 2. DESCRIPTION OF THE PROCESS CHAIN

The process chain currently under development is displayed in Figure 1. Starting from an easy to manufacture glass preform, a first processing step removes redundant material with high speed laser ablation. A second step polishes the resulting surface and reduces the roughness generated from the High Speed Laser Ablation step without removing any material. An optional third step locally removes remaining redundant material with high precision and leads to the desired freeform optics. During and/or between these steps, a measuring of the geometry and shape accuracy is executed in order to match the actual with the targeted result.

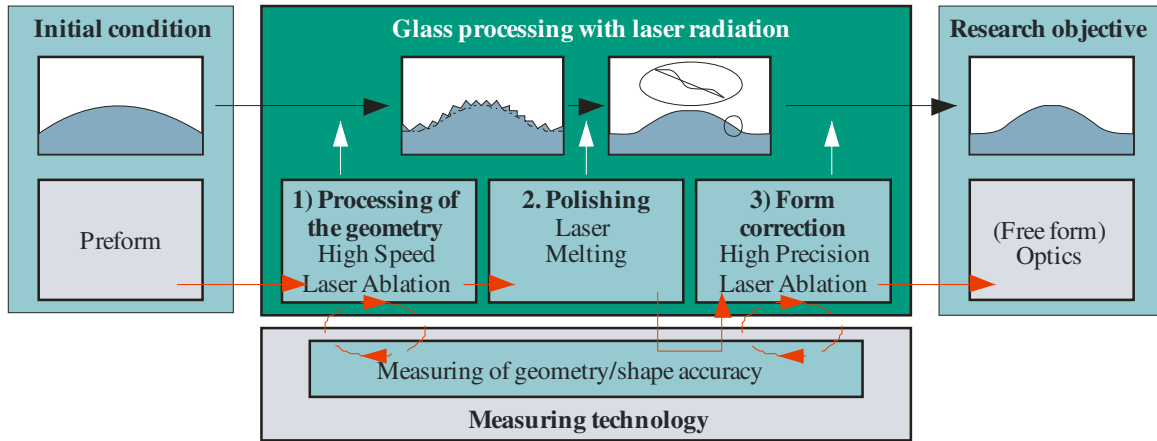


Figure 1. Laser based process chain for manufacturing free form optics

Compared to conventional manufacturing methods, one great advantage of this process chain is the decoupling of tool and work piece geometry, leading to a great amount of flexibility and a short processing time, which is nearly independent of the surface geometry, but only varies with the optics size and the amount of material to be removed. Moreover, no additives like cooling liquids or abrasives are required, so the costs decrease and the environment is protected.

In the following, the three laser based process steps are described in more detail.

### 2.1 High Speed Laser Ablation

The aim of the first process step is the fast removal of redundant glass material from the preform and the creation of the desired optics shape. For this purpose, high laser powers are used to heat up and vaporize the glass surface. The resulting glass vapor is removed from the working area with an extraction system so that it neither can affect the ablation process by absorption of the laser energy nor damage the surrounding components by condensation.

The scan strategy, which describes the movement of the laser beam over the glass surface, is of significant importance because it strongly influences the resulting surface roughness. One scan strategy is displayed in Figure 2.

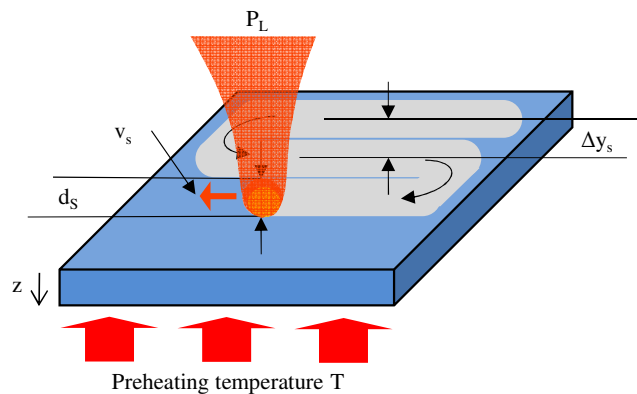


Figure 2. Schematic description of the High Speed Laser Ablation step

There, the laser beam with the laser power  $P_L$  and the focus diameter  $d_s$  is moved over the glass sample in a meandering path with the scan speed  $v_s$  and the track pitch  $\Delta y_s$ . To reduce thermal stresses inside the glass material, it is preheated to the temperature  $T$ . Together with the number of exposure layers  $n$  and the measurement of the ablation depth  $z$ , these parameters can be used to determine the ablation rate  $\dot{V}$  which describes the amount of ablated glass material in a certain time. In order to reach a short processing time, a high ablation rate is aspired for the High Speed Laser Ablation process.

$$\dot{V} = \frac{z * \Delta y_s * v_s}{n} \left[ \frac{mm^3}{s} \right] \quad (1)$$

According to the formula, a high ablation rate can be achieved by either increasing the ablation depth, the track pitch and the scan speed or decreasing the number of exposure layers. Nevertheless, these parameters have to be chosen accordingly, so that the resulting surface roughness still remains on a low level. An overview is given in Chapter 4.1.

## 2.2 Laser Polishing

Compared to the High Speed Laser Ablation step, the Laser Polishing step uses a different scan strategy which is displayed in Figure 3. On an equally preheated test glass sample, the laser beam is used defocused for a more homogenous energy distribution and moved in one axis at high speed  $v_s$  to create a working line instead of a working spot. This line with the width  $b_{Line}$  is moved forward at the speed  $v_{feed}$  and uniformly heats up the glass material just below its vaporization point. Thereby, the viscosity is reduced and the initial roughness smoothens because of the surface tension. In this process step, no material is ablated and the surface shape remains unchanged.

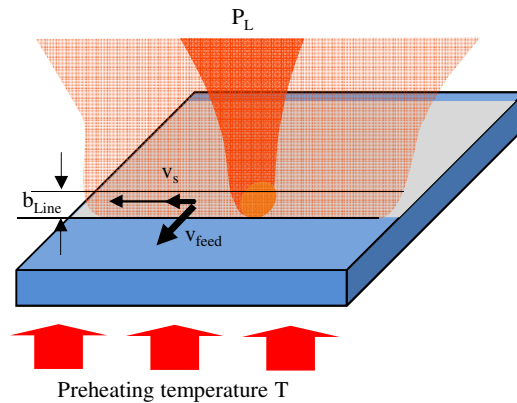


Figure 3. Schematic description of the Laser Polishing step

The temperature of the glass has to be controlled very precisely to avoid material ablation at temperatures above the vaporization point of the material as well as an increasing viscosity and thus a higher remaining surface roughness at lower temperatures. This is realized with a pyrometer that controls the surface temperature of the processed glass by adjusting the laser power accordingly. Moreover, it is important for the Laser Polishing step that the glass surface is free of particles before processing. Because of the high temperatures during processing, any remaining particle is burnt into the surface and leads to a higher resulting roughness. To ensure a clean surface, the glass samples are cleaned before polishing and the laser machine used is encased with a flowbox which reduces the amount of dust particles through filtration. An overview is given in Chapter 4.2.

## 2.3 High Precision Laser Ablation

The aim of the High Precision Laser Ablation step as the last step of the process chain is to remove remaining redundant material. Therefore, a high spatial resolution combined with a small ablation depth is needed. To reach this, the same scan strategies as for the High Speed Laser Ablation step are used (see Figure 2), but here, not the ablation rate  $\dot{V}$ , but the energy density per layer  $E_A$  is of great importance.

$$E_A = \frac{P_L}{\Delta y_s * v_s} \left[ \frac{J}{mm^2} \right] \quad (2)$$

According to this formula, lower surface energies and thus smaller ablation depths can be reached with a decreased laser power and an increased scan speed or track pitch. If the energy density decreases below the value which is needed to vaporize the glass material, no material is ablated but only heated, and the surface remains unchanged. So, the ablation depth can be adjusted by varying at least one of the process parameters mentioned. Again, the parameters have to be chosen accordingly, in order to achieve a low surface roughness. An overview is given in Chapter 4.3.

### 2.4 Combination of the process steps and alternative laser sources

If possible, all process steps should be conducted with the same laser source in order to reduce the investment costs. A high power CO<sub>2</sub> laser source with a wavelength of  $\lambda = 10.6 \mu\text{m}$  and its high absorption on the glass surface is compulsory for the Laser Polishing step due to the surface temperature needed, and so it is favored for the two ablation steps as well. A combination of the first two process steps is given in Chapter 4.4. In addition, ablation experiments are carried out using an ultra short pulse laser, which uses different effects for the ablation process [2]. The results of experiments carried out with this laser source as well as a comparison with the results of the CO<sub>2</sub> laser ablation are given in Chapter 4.5.

## 3. EXPERIMENTAL SETUP AND ANALYSIS PROCEDURE

In this chapter, the basic experimental setup with a CO<sub>2</sub> laser source, the glass material used for the experiments and the analysis procedure applied to the produced test geometries are described.

### 3.1 Experimental setup

The experimental setup which is used for the development of the presented process chain is displayed in Figure 4. The whole installation is surrounded by a Flowbox which filters the air in order to prevent dust particles from settling on the glass surface during the laser treatment. The experiments are carried out with a 1.5 KW CO<sub>2</sub> laser. A laser scanner, which is mounted on two axes, is used to position and move the laser beam on the glass surface at a maximum scan speed of  $v_s = 10 \text{ m/s}$ . The attached ZnSe lens focuses the laser beam to a minimum diameter of  $d_s = 450 \mu\text{m}$  with a Gaussian intensity profile. The glass itself is heated up with a heating plate for lowering the temperature difference as well as the temperature gradient and thus the residual stress during laser processing. An extraction system in combination with a cross-jet is used to remove vaporized glass from the processing area.

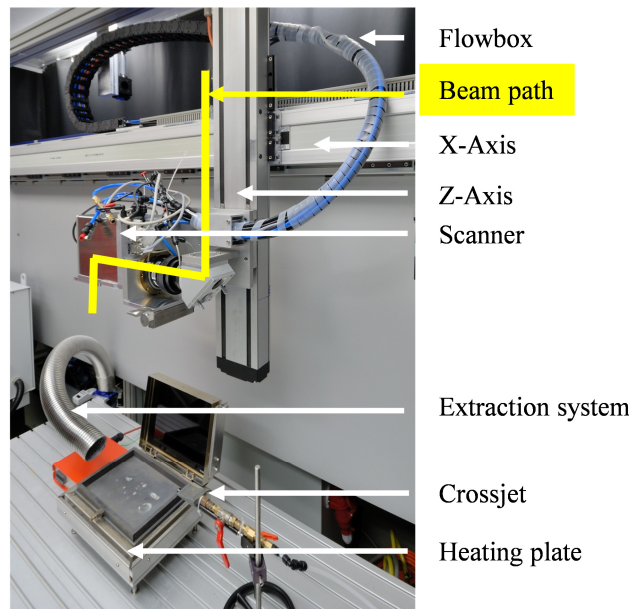


Figure 4. Experimental setup

For the Laser Polishing step, a pyrometer can be attached to the experimental setup in order to measure the sample surface's temperature and, thereby, adjust the laser power accordingly. Moreover, different setups are available, including a positioning system for the glass samples with an integrated extraction system, and several ovens which allow higher preheating temperatures and tempering processes.

### 3.2 Glass material

For the experiments, polished square plates of fused silica with an edge length of 80 mm, a thickness of 3 mm and a surface roughness of  $R_a = 2 \text{ nm}$  are used. The combination of the first two process steps is demonstrated on square plates with an edge length of 20 mm, a thickness of 5 mm and a ground surface. Regarding the processing with laser radiation, the low thermal expansion coefficient of  $\gamma \approx 6 \cdot 10^{-7} \text{ 1/K}$  as well as the low thermal conductivity of  $\kappa \approx 2.7 \text{ W/(K}\cdot\text{m)}$  of fused silica are advantages compared to other types of glass [3]. Its absorption, reflection and transmission coefficients for different wavelengths  $\lambda$  are displayed in Figure 5. About 80% of the  $\text{CO}_2$  laser radiation with a wavelength of  $\lambda = 10.6 \text{ }\mu\text{m}$  is absorbed and the rest is reflected, leading to a high efficiency.

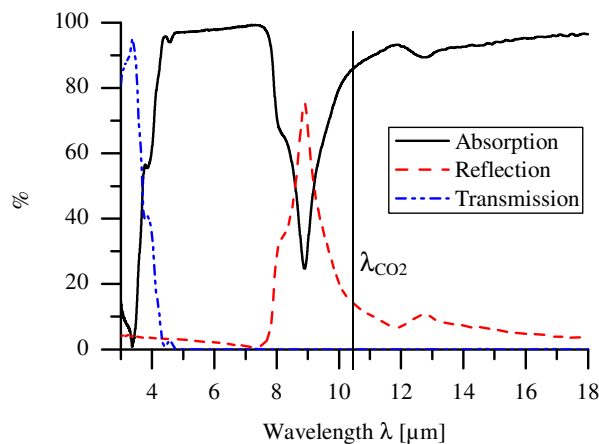


Figure 5. Absorption, reflection and transmission of fused silica as a function of the wavelength

To reduce thermal stresses which are induced during laser processing and that can lead to double refractions, the glass samples are subsequently tempered. Thereby, the glass samples are heated up above their lower relaxation temperature ( $T \approx 1050 \text{ }^\circ\text{C}$  for fused silica [3]) and slowly cooled down afterwards. During the temper process, the surface shape remains unchanged.

### 3.3 Analysis procedure

To determine the influence of the process parameters on the ablation depth and the resulting surface roughness of the process chain's ablation steps, rectangular test fields with a dimension of  $10 \times 10 \text{ mm}^2$  are ablated with systematically varied parameter settings. The ablation depth  $z$  and the resulting surface roughness of the ablated test fields are measured by using white light interferometry. This method offers the advantage of a two-dimensional data recording with a high spatial resolution in one measurement.

The analysis procedure is shown in Figure 6. First, the surface roughness is measured in the middle of the ablated field in an area of  $2 \times 1 \text{ mm}^2$ . As can be seen, a much higher ablation depth is reached at the edges of the field due to the reversal points and the higher temperature in this area. The ablation depth is determined with the measurement of an unablated area on the glass sample and a height comparison between the ablated and unablated field. In Figure 6, the entire area around the ablated field is used as this reference surface.

The measurement error of this evaluation is below 1% for both ablation depth as well as surface roughness. For example, a measured ablation depth of  $z = 500 \text{ }\mu\text{m}$  varies about  $\pm 1.8 \text{ }\mu\text{m}$  when moving the measurement area across the ablated field. The corresponding surface roughness of  $R_a = 5.3 \text{ }\mu\text{m}$  varies about  $\pm 0.05 \text{ }\mu\text{m}$ . Thus, this analysis procedure is sufficiently accurate.

When analyzing a laser-polished test sample, the surface roughness is identified in the same way, but on a larger area. The measurement of the ablation depth is not necessary due to the fact that the Laser Polishing step only remelts the surface and does not ablate material. In addition, the roughness of single wavelengths is calculated in order to compare

the influence of different process parameters in more detail. This is done by a fast Fourier transformation of the measured surface data. Its results are displayed and discussed in Chapter 4.2.

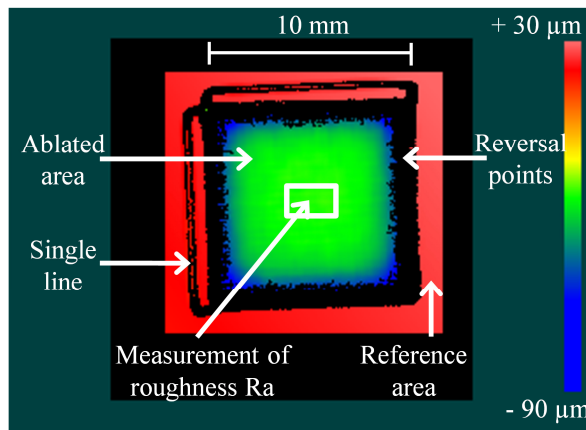


Figure 6. Identification of the surface roughness and the ablation depth

## 4. RESULTS

To determine suitable process parameters, each process step is developed separately. In this chapter, the results of the single process step are presented, as well as a first combination to the described process chain. Moreover, the results of glass processing with ultra short pulse laser radiation are presented.

### 4.1 High Speed Laser Ablation

In order to reach a high ablation rate and, thus, a short processing time, experiments are conducted with high laser powers which then lead to high ablation depths. The resulting ablation rate as well as the corresponding surface roughness of ablated fields with alternating scan speeds and track pitches is displayed in Figure 7. For these experiments, the maximum laser power of  $P_L = 1.5$  KW and  $n = 8$  exposure layers are used with the meander scan strategy.

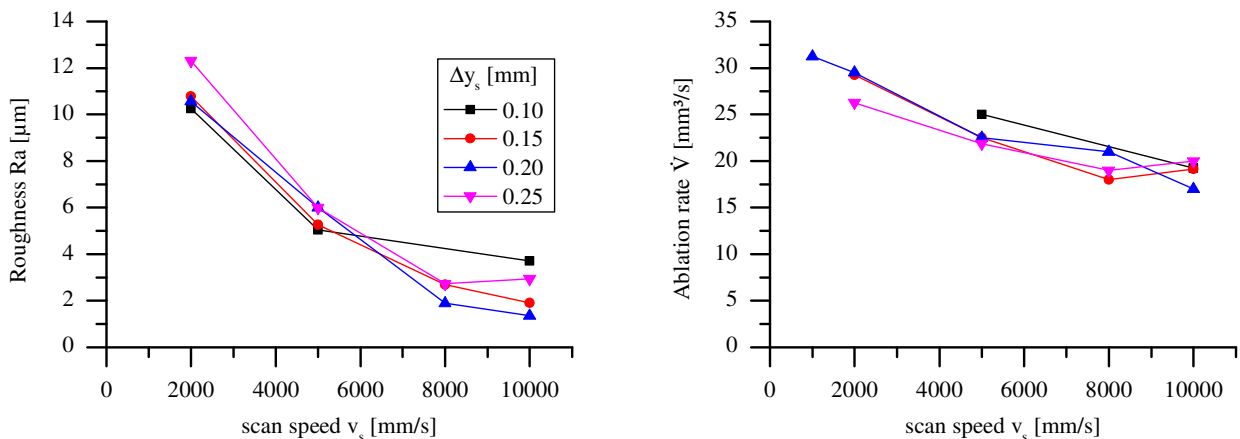


Figure 7. (a) Ablation rate and (b) surface roughness of test samples treated with High Speed Laser Ablation

For all parameters, an ablation rate  $\dot{V} \geq 18$  mm³/s can be achieved. This example is representative for all experiments conducted with high laser power in order to achieve high ablation rates. Due to a lower energy density  $E_A$  and therefore a lower ablation depth  $z$ , the surface roughness is reduced with increasing scan speeds. At a scan speed of  $v_s = 2000$  mm/s, a roughness of  $Ra \approx 11$  μm is achieved, at  $v_s = 10.000$  mm/s, the roughness accounts to  $Ra \approx 3$  μm. Furthermore, a track pitch of  $\Delta y_s = 0.2$  mm reaches the lowest roughness. The surface roughness can be further decreased when optimizing the experimental setup as well as the scan strategy, which will be discussed in the following chapter.

#### 4.1.1 Reduction of surface roughness

Due to a smaller absorption of the laser radiation above the test sample and thus a more uniform process, an effective removal of the ablated glass vapor leads to a lower surface roughness. For this, the extraction system has been modified and moreover integrated into a glass positioning system, which allows a smaller distance between the working area and the extraction system and thus a better removal of the glass vapor. With this optimization, the surface roughness can be significantly lowered, especially for the rather slow scan speeds. For  $v_s = 1000$  mm/s, the surface roughness decreases from  $R_a = 25$   $\mu\text{m}$  to  $R_a = 10$   $\mu\text{m}$ . Compared to Figure 7, this surface roughness is smaller than the initial surface roughness gained with  $v_s = 2000$  mm/s. The difference between the results decreases towards higher scan speeds, but still remains distinct.

Using an optimized scan strategy also lowers the resulting surface roughness. One disadvantage of the meander scan strategy is the high ablation depth at the reversal points (see Figure 2). This is caused by the changing of the scan direction and the delay of the scanner mirrors because of de- and acceleration during this action. Moreover, due to the small track pitch, the next line directly crosses an area which is still heated up from the previous line, so the ablation depth increases even more. In addition, experiments show that the ablation depth varies depending on the scan direction relative to the cross-jet and extraction system. Therefore, using a unidirectional scan strategy as it is shown in Figure 8 (left) offers many advantages. As displayed, the scan direction remains constant for one exposure layer and the laser is moved back to the starting side outside the sample field in order to avoid having to turn the laser off and on again which would cause oscillations in the laser power. As shown in Figure 8 (right), the unidirectional scan strategy leads to a lower surface roughness when comparing fields with the same ablation depth. In spite of its movement of the laser beam outside the ablation field, it reaches nearly the same efficiency as the meander scan strategy due to the allotted turning points and is thereby preferred.

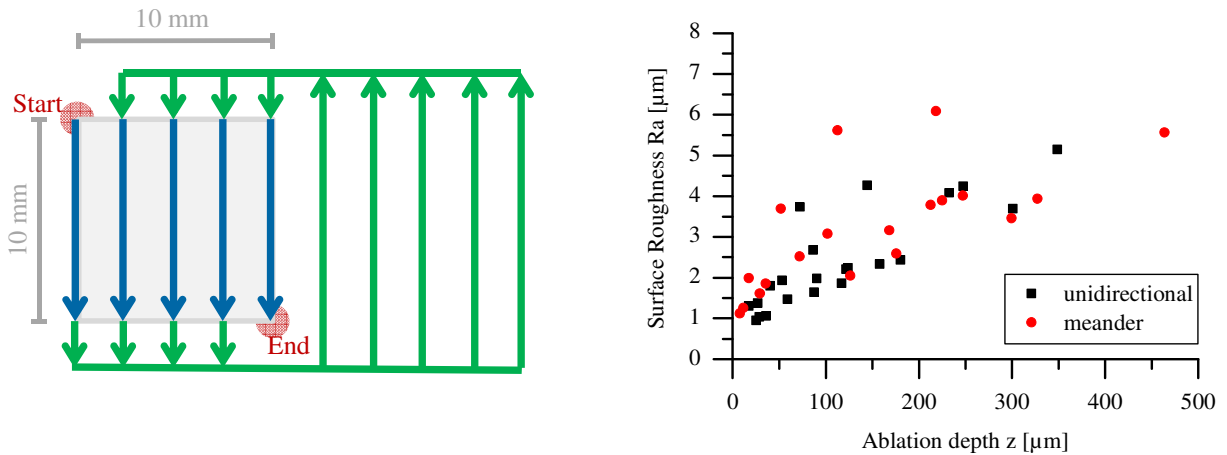


Figure 8. (a) Schematic drawing of one layer with a unidirectional scan strategy and (b) comparison of the resulting surface roughness of two different scan strategies

#### 4.1.2 Mutable ablation depth for non-planar surfaces

Due to a smaller energy density  $E_A$ , it is obvious that the ablation depth decreases towards higher scan speeds. Hence, this makes it possible to locally alter the amount of ablated material and thus form a surface shape solely by changing the scan speed. Compared to a variation of the laser power  $P_L$ , which can also be used to alter the ablation depth, this method is both faster because of the shorter reaction time of the scanner system as well as more efficient due to the high ablation rates at constant high laser powers. Compared to a variation of the ablation depth by locally using different numbers of exposure layers, the scan speed variation offers the advantage of continuous rather than discrete ablation depths. Moreover, the number of settling processes of the laser source is reduced to just one when using the unidirectional scan strategy (see Figure 8 left).

The dependency between scan speed and ablation depth per layer is displayed in Figure 9 for  $P_L = 1.5$  KW,  $\Delta y_s = 150$   $\mu\text{m}$ .

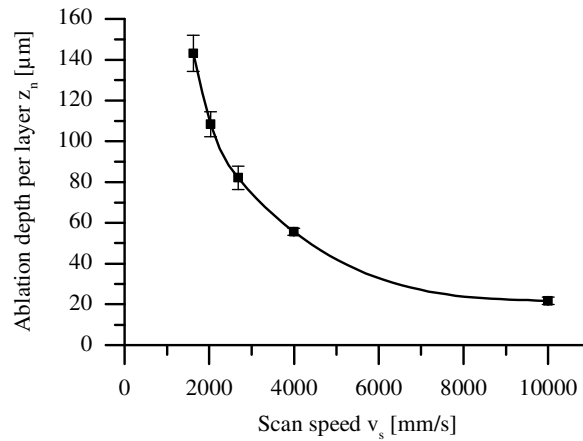


Figure 9. Ablation depth per layer over scan speed for the High Speed Laser Ablation step

The dependency shown between scan speed and ablation depth can be approximated using the following formula:

$$z = \frac{A_1 - A_2}{1 + \left(\frac{v_s}{v_0}\right)^p} + A_2 \quad (3)$$

with

$$\begin{aligned} A_1 &= 410.23 \mu\text{m} \\ A_2 &= 6.32 \mu\text{m} \\ v_0 &= 1071.11 \text{ mm/s} \\ p &= 1.6694 \end{aligned}$$

With this formula, it is possible to locally ablate different amounts of glass material and thus form the desired surface shape. Basic limitations regarding spatial resolution are the focus diameter, the ablation depth even with highest scan speeds and the response time of the scanner system. As an example, Figure 10 shows a graphical illustration of a unidirectional scanner script with colored and height-adjusted scan speeds and the resulting surface after High Speed Laser Ablation with a processing time of  $t \approx 30$  s.

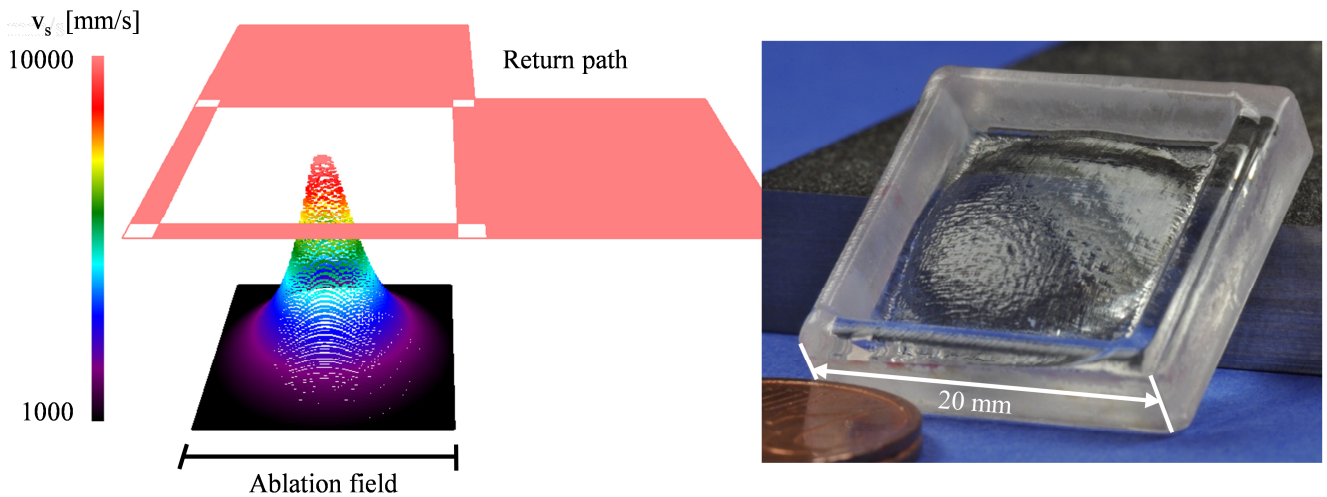


Figure 10. (a) Graphical illustration of a unidirectional scan strategy and (b) processed surface through High Speed Laser Ablation

Besides processing the spherical surface shown, this technique can be used to manufacture freeform surfaces as well simply by adapting the scan speed to the desired surface shape.

## 4.2 Laser Polishing

By heating up the glass surface and thus lowering its viscosity, the Laser Polishing step is able to significantly reduce the surface roughness [4]. To achieve best results, the laser beam is used defocused which leads to a larger working area and a more homogeneous energy distribution. With an intensity of  $400 \text{ W/cm}^2$ , an area rate of about  $1 \text{ cm}^2/\text{s}$  can be achieved, which is fast compared to conventional polishing. The working area exceeds the sample dimensions so that the reversal points can be placed outside the sample because of the higher temperatures and the risk of an unwanted material ablation in this area.

During the process development, the Laser Polishing step is examined on test samples with a flat ground surface in order to reduce the number of variables that may influence the resulting surface roughness. A detailed look at the achieved results is given in Figure 11, where the surface roughness of conventional and laser-polished surfaces is compared above the spatial wavelengths  $\lambda$  of the roughness. Starting from a ground surface, the laser polishing process already reaches a better surface roughness than conventional methods for spatial wavelengths  $\lambda < 100 \mu\text{m}$ . A problem remains in the longer wavelengths  $\lambda > 100 \mu\text{m}$ , where the roughness of the laser-polished surface increases significantly. Although this result is not acceptable for imaging optics, it is already sufficient for lighting optics.

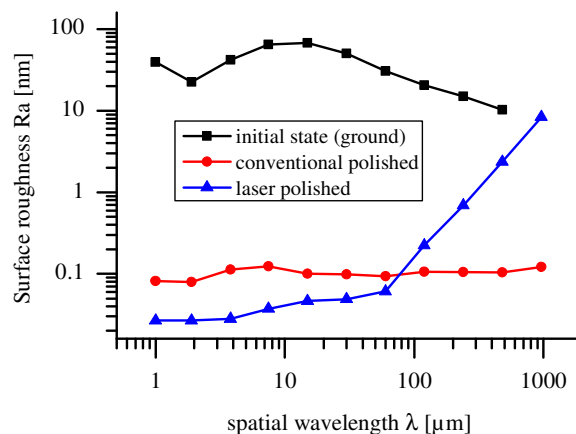


Figure 11. Initial state, conventional and laser-polished surface roughness as a function of the spatial wavelength

To transfer the identified process parameters to samples with a curved surface, several adaptations have to be conducted. For example, the surface area covered of the laser spot increases when polishing with an angle different from  $\beta = 0^\circ$  between the laser beam and the surface normal, leading to decreased energy density. A schematic drawing of this correlation is displayed in Figure 12. To compensate this effect, either an adaption of the laser power or of the scan speed can be used.

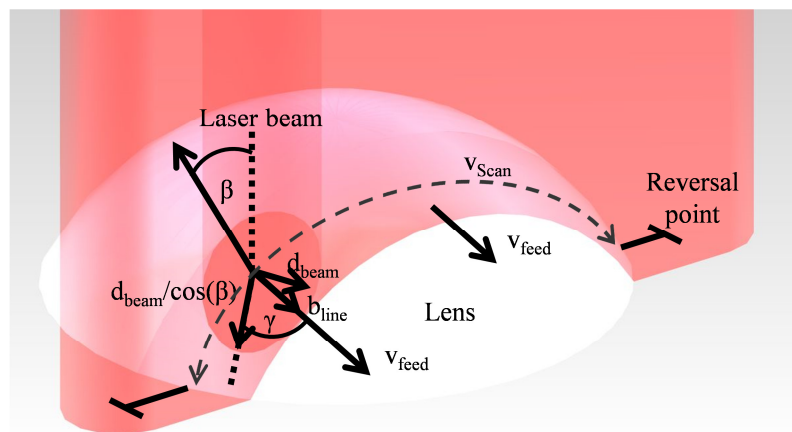


Figure 12. Schematic drawing of the process parameters adaption due to the non-planar optics surface

Another point to consider is the temperature distribution of the optics during processing. Towards the end of the Laser Polishing step, the optics is heated up due to the previous processing. In order to avoid material ablation through surface temperatures above the ablation temperature, the laser power is decreased. The identification of suitable process parameters for this adaption is carried out with a thermal imaging camera.

With these and other adaptations, nearly every surface form, including aspheres and free form optics, can be laser-polished. As an example, Figure 13 displays a spherical optics with ground surface as initial state (left) and laser-polished (right). The processing time for this Laser Polishing step is  $t_{\text{polishing}} < 25$  s. Compared to conventional polishing, this means a reduction of processing time by at least a factor of 10 and even more if the optics shape is nonspherical.

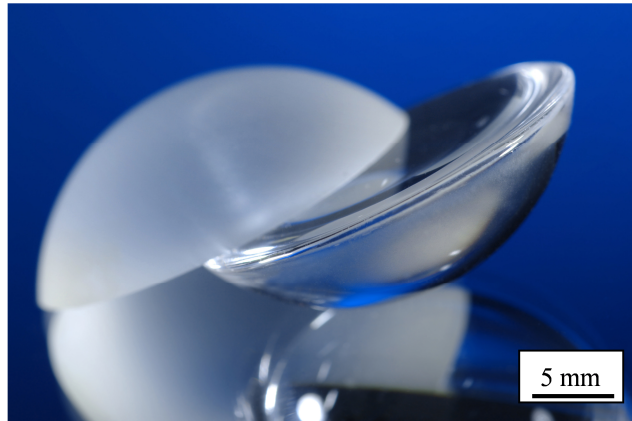


Figure 13. Initial state (ground) and laser-polished spherical lens

More information about the Laser Polishing step can be found in [4,5].

### 4.3 High Precision Laser Ablation

Due to the demands to e.g. imaging optics, the remaining surface roughness in the longer wavelengths  $\lambda > 100 \mu\text{m}$  has to be removed. Beneath several optimizations in the Laser Polishing step, the High Precision Laser Ablation step shall be used to locally ablate small amounts of redundant glass material in order to reduce the waviness. So, this High Precision Laser Ablation step aims for ablation depths  $\ll 100$  nm with a spatial resolution  $< 100 \mu\text{m}$  and minimal resulting surface roughness. Therefore, the laser power is decreased in comparison to the High Speed Laser Ablation step in order to reduce the ablation depth. The dependency between the scan speed and the ablation depth, which is already displayed in Figure 9, is also valid for this ablation step, with smaller ablation depths reached for the same scan speeds. This dependency again can be used to locally alter the ablation depth in order to remove material where wanted. An example is displayed in Figure 14, where a wave-shaped surface is generated through varying the scan speeds.

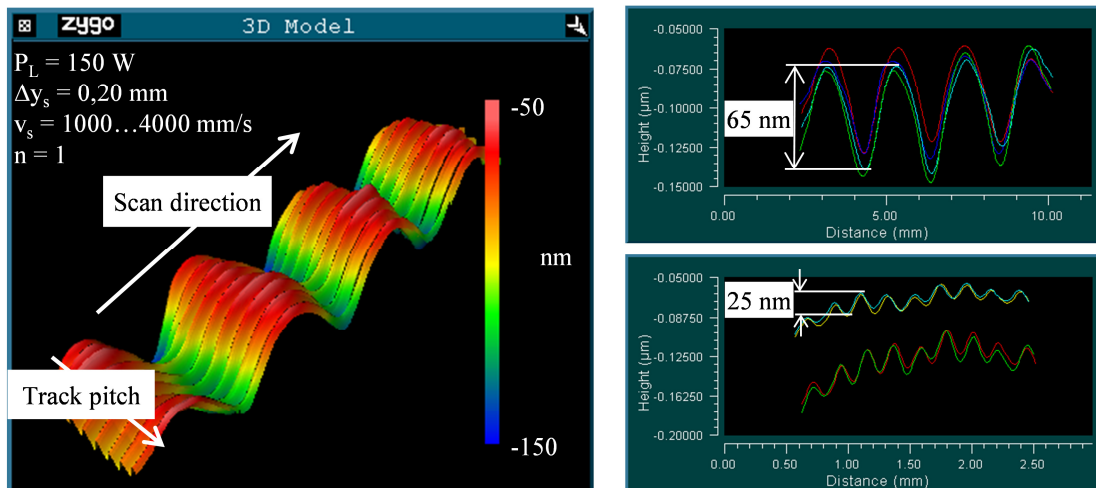


Figure 14. White light interferometer record of a surface generated by locally varied scan speeds and ablation depth s

Due to the high scan speeds used and the response time of the scanner system, the spatial resolution is not yet sufficient. In order to increase the spatial resolution, the scan speed and the laser power are decreased simultaneously, leading to a constant energy density  $E_A$  and, thus, a remaining small ablation depth. The results of these adjusted parameters are displayed in Figure 15. On the left side, a test field with constant parameters is ablated, which results in a surface roughness  $R_a \approx 2.3$  nm (initial surface roughness  $R_a = 2$  nm) and an ablation depth of  $z = 17$  nm for 12 exposure layers. The processing time for this ablation field amounts to  $t = 48$  s. On the right side, two different scan speeds are used to locally ablate material. In this case, the higher scan speed does not ablate any material at all because of a energy density below the needed threshold.

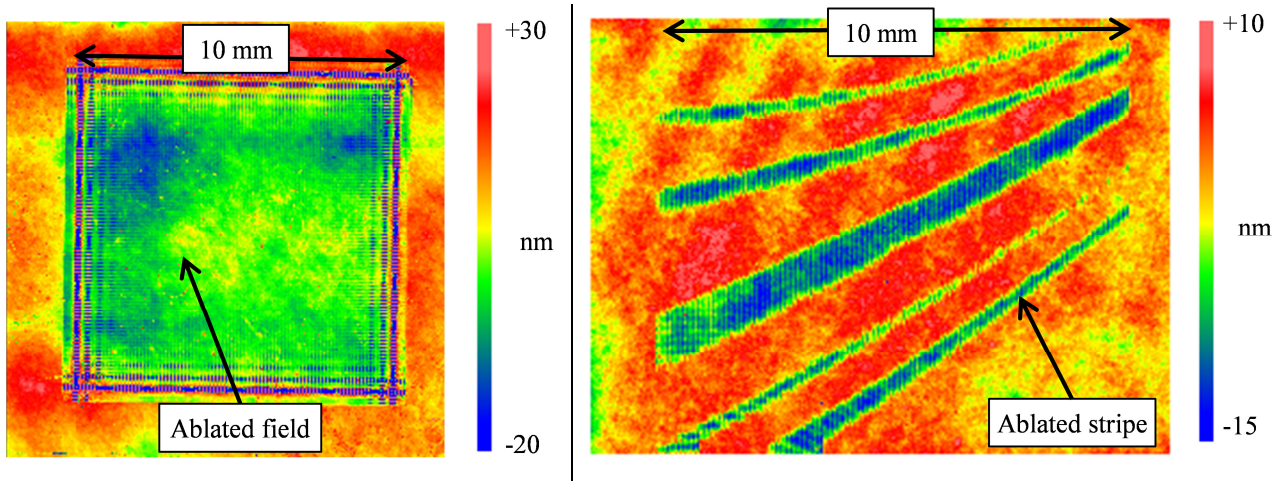


Figure 15. Ablated test field with constant (left) and altered (right) scan speeds.

The spatial resolution achieved is about  $200 \mu\text{m}$  in scan direction which is not yet sufficient but can be increased further using smaller scan speeds and laser powers. Moreover, every described enhancement to improve the High Speed Laser Ablation step in Chapter 4.1 is also valid here.

#### 4.4 Combination of the process steps

A first example of the High Speed Laser Ablation step in combination with the Laser Polishing step is given in Figure 16. There, starting from a ground block of fused silica with an edge length of 20 mm and a plane surface, a cylinder lens array is formed with the High Speed Laser Ablation step (1). The following Laser Polishing step reduces the surface roughness on the front side (2a) and on the rear side (2b).

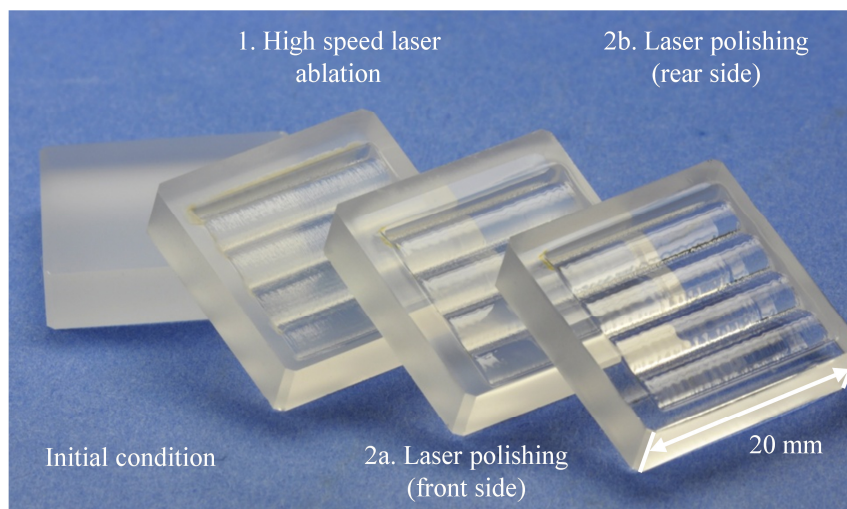


Figure 16. Demonstration of the combination of the single steps towards the process chain

It can be seen that the resulting test piece is optically transparent, although it does not yet exhibit a sufficient surface roughness and shape accuracy. One reason for that is the not yet optimized connection between the process steps, another one is the not applied High Precision Laser Ablation step. For this, the test piece has to be measured offline in order to identify the position of the remaining waviness and then put back into the experimental setup for further treatment. This step has not been executed yet.

#### 4.5 Ultra Short Pulse Laser Ablation

Despite its transparency at wavelengths of the near infrared, an ablation of fused silica is also possible with ultra short pulse laser radiation at  $\lambda \approx 1 \mu\text{m}$  due to multi-photon-absorption [3]. Experimental results achieved with an ultra short pulse laser ( $\lambda = 1030 \text{ nm}$ ) provided by AMPHOS [6] are shown in this chapter.

Compared to the results of the experiments conducted with  $\text{CO}_2$  laser radiation, one advantage of the described ultra short pulse laser is its small focus diameter and the consequential high spatial resolution. A single ablated line with 4 exposure layers is shown in Figure 17. It can be seen that an ablation width of  $25 \mu\text{m}$  and an ablation depth of  $3.72 \mu\text{m}$  are achieved. The ablation depth can be further reduced by decreasing the number of exposure layers or the laser power.

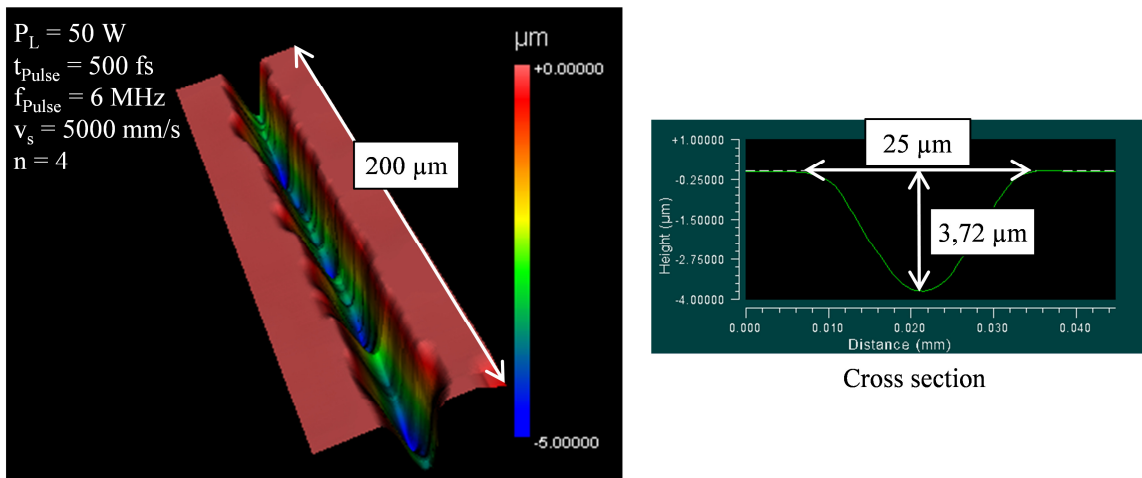


Figure 17. Single ablated line with ultra short pulse laser

When several single lines are ablated close to each other, a connected surface can be ablated. Results of such experiments with a laser power of  $P_L = 160 \text{ W}$ , a pulse duration of  $t_p = 500 \text{ fs}$ , a focus diameter of  $d_s = 22 \mu\text{m}$  and 20 layers, addressing the High Speed Laser Ablation step, are displayed in Figure 18.

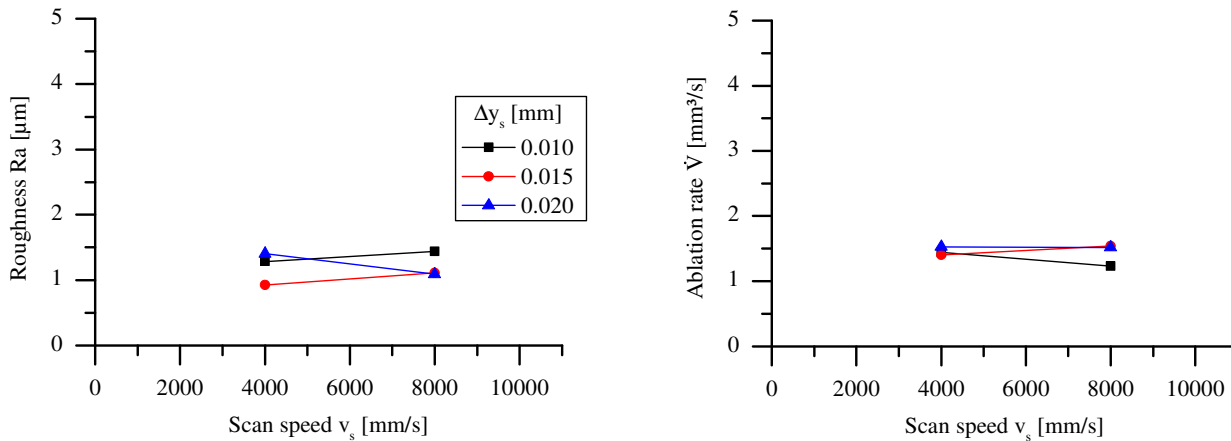


Figure 18. (a) Ablation rate and (b) surface roughness of test samples treated with ultra short pulse laser radiation ( $P_L = 160 \text{ W}$ ,  $n = 20$ )

There, the surface roughness amounts to  $Ra = 0.9 \mu\text{m}$  and  $Ra = 1.5 \mu\text{m}$  and the ablation rate reaches about  $\dot{V} = 1.5 \text{ mm}^3/\text{s}$  regardless of the parameter setting. Compared to the results of the ablation experiments carried out with  $\text{CO}_2$  laser radiation (see Chapter 4.1), the results achieved with ultra short pulse laser ablation do not reach the high ablation rate of the High Speed Laser Ablation step due to its lower laser power. Nevertheless, it can be used for this process step when only small amounts of material have to be ablated.

In Figure 19, the resulting surface roughness of the ultra short pulse laser ablation and of the High Speed Laser ablation with  $\text{CO}_2$  laser radiation is compared as a function of the spatial wavelengths  $\lambda$ . In addition, the roughness of the initial condition as well as a conventional ground glass surface with a grain size of  $9 \mu\text{m}$  is displayed.

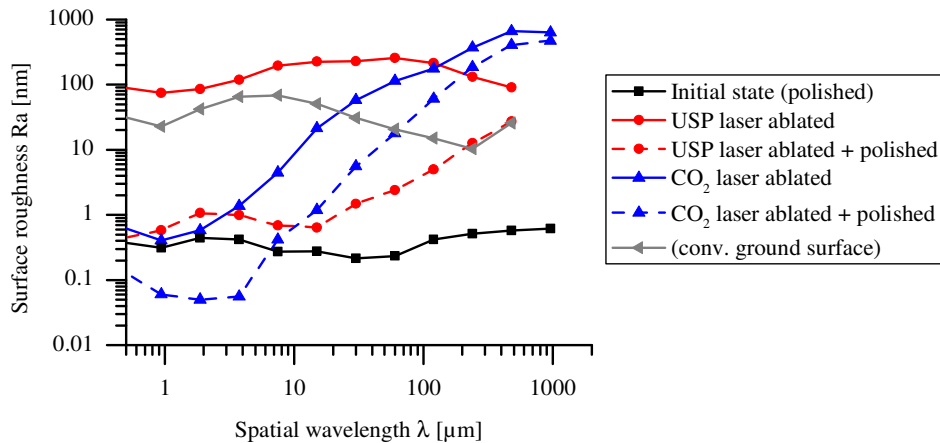


Figure 19. Surface roughness  $Ra$  of ultra short pulse and  $\text{CO}_2$  laser ablation as a function of the spatial wavelength

It can be seen that the  $\text{CO}_2$  laser ablation reaches a lower roughness than the ultra short pulse laser ablation for wavelengths  $\lambda < 100 \mu\text{m}$ . This is caused by the thermal heating during the  $\text{CO}_2$  laser ablation process which remelts the unablated surrounding glass material locally and thus smoothens the surface. For wavelengths  $\lambda > 100 \mu\text{m}$ , the surface roughness increases significantly, whereas the surface roughness of the test field ablated with ultra short pulse laser radiation shows a more homogenous roughness distribution at the examined spatial wavelengths. When the Laser Polishing step is conducted on the ablated fields, the surface roughness of both fields strongly decreases for small wavelengths to values near or even below the initial state. For longer wavelengths, the surface roughness of the field ablated with ultra short pulse laser radiation is reduced further than the surface roughness of the field ablated with  $\text{CO}_2$  laser radiation.

It has to be noted that neither the compared ablated fields nor the Laser Polishing step is optimized towards each other, so these results may not be universally valid. But when considering the ability of the polishing process to effectively remove spatial wavelengths below  $\lambda < 100 \mu\text{m}$  which is already shown in Figure 11, the ultra short pulse laser ablation is well suited for the ablation requirements of glass material and offers several different characteristics compared to the ablation with  $\text{CO}_2$  laser radiation. To finally answer the qualification of the ultra short pulse laser ablation within the presented process chain, more experiments have to be conducted.

## 5. SUMMARY

The current development of a laser based process chain for optics manufacturing is presented. Starting from a preform, this process chain is based on the three individual process steps High Speed Laser Ablation, Laser Polishing and High Precision Laser Ablation, which are used to manufacture the desired optics. In this paper, the main procedure with the relevant process parameters as well as results of each process step regarding surface roughness and ablation rate are presented for fused silica.

Using  $\text{CO}_2$  laser radiation, The High Speed Laser Ablation step is capable of ablating glass material with an ablation rate of  $\dot{V} \geq 20 \text{ mm}^3/\text{s}$ , leading to a short processing time. Starting from a conventionally ground surface, the Laser Polishing step reduces the surface roughness to values that are already sufficient for lighting optics and only needs a fraction of

time required by conventional polishing methods. The High Precision Laser Ablation step ablates the smallest amounts of glass material with high vertical spatial resolution. Finally, a first combination of the first two process steps towards the process chain already shows promising results.

In addition to experiments conducted with CO<sub>2</sub> laser radiation, using ultra short pulse laser radiation for the ablation steps is investigated as well. Due to the smaller laser power, a lower ablation rate of  $\dot{V} \approx 1.5 \text{ mm}^3/\text{s}$  is achieved, but the lateral spatial resolution is much higher because of the smaller focus diameter.

## 6. CONCLUSION AND OUTLOOK

By replacing conventional with laser based manufacturing methods, this approach offers advantages concerning processing speed, individualization and especially flexibility regarding the optics' surface shape, and thereby paves the way for manufacturing nonspherical or even free form optics without any needed extra time. The experimental results show that it is possible to both ablate and polish fused silica with CO<sub>2</sub> laser radiation in a time which is interesting for industrial applications. Due to the fact that the single process steps can also be used individually, other applications, such as surface structuring or polishing within drilling holes, can be addressed as well.

The next step will be the combination of the single process steps towards the process chain, including the development of suited interfaces between the single steps. For this, in addition to suited process parameters, an online measurement system has to be identified and installed into the experimental setup in order to combine the single steps and to reduce the down time. With this setup, several different geometries, including free form optics, will be manufactured and examined.

## 7. ACKNOWLEDGEMENTS

Parts of this work have been conducted within the FoPoLas project which is supported by the Federal Ministry of Education and Research (BMBF) and the project executing organization VDITZ. The polishing step is based on the developments within the PoliLas project which was supported by the Federal Ministry of Economics and Technology (BMWi) and the project executing organization VDI/VDE-IT.

## 8. REFERENCES

- [1] Bliedtner, J. and Gräfe, G., [Optiktechnologie - Grundlagen, Verfahren, Anwendungen, Beispiele] Hanser Fachbuchverlag, München, (2008)
- [2] Perry, M.D., Stuart, B.C., Banks, P.S., Feit, M.D., Yanovsky, V. and Rubenchik, A.M., "Ultrashort-pulse laser machining of dielectric materials," Journal of applied physics 85, 6803-6810 (1999)
- [3] Heraeus, Data sheet fused silica, Heraeus Holding GmbH, Hanau, Dec. 03 2011.
- [4] Richmann, A., Willenborg, E. and Wissenbach, K., "Laser polishing of spherical quartz lenses," Manufacturing of optics, Munich (2011)
- [5] Richmann, A., Willenborg, E. and Wissenbach, K., "Laser polishing of fused silica," Optical fabrication and testing (OF&T), Jackson Hole (2010)
- [6] AMPHOS GmbH, Steinbachstr. 15, 52074 Aachen, Germany, <http://www.amphos.de>